Journal of Materials Chemistry A

RSC Publishing

PAPER

View Article Online
View Journal | View Issue

Cite this: J. Mater. Chem. A, 2013, 1, 3797

Novel DLC/ionic liquid/graphene nanocomposite coatings towards high-vacuum related space applications

Xiufang Liu,[ab] Jibin Pu,[a] Liping Wang*[a] and Qunji Xue[a]

Received 19th October 2012
Accepted 11th January 2013

DOI: 10.1039/c3ta00764b

www.rsc.org/MaterialsA

It is currently a challenge for space tribology to develop a long lifetime and high bearing capacity lubricant meeting the requirements of space applications. Herein, we dispersed graphene into ionic liquid, prepared novel composite coatings of diamond-like carbon (DLC)/ionic liquid (IL)/graphene with different graphene concentrations, and investigated its space performance under high vacuum and space radiation conditions. IL/graphene nanofluids with different concentrations were examined by Fourier transform infrared spectroscopy (FTIR). Furthermore, IL/graphene nanofluids after friction tests were investigated by X-ray photoelectron spectroscopy (XPS), and high-resolution transmission electron microscopy (HRTEM). The results showed that the graphene concentration would obviously affect the spatial tribology performance of the composite coatings. Because the excess graphene in the IL would tend to form irreversible agglomerates, leading to reduction of the effective graphene dose, an optimum graphene concentration (0.075 mg ml^{-1}) in IL for the composite coatings was required to exhibit the lowest friction coefficient, the highest bearing capacity and the strongest anti-irradiation in a simulated space environment. In addition, XPS spectra further confirmed that the formation of a fluorinated oil-containing carbon-rich tribofilm between the friction pairs further ensured the good antifriction and wear resistance performance of DLC/IL/graphene.

1 Introduction

The lifetime of lubricants is a key factor for space exploration. Due to the harsh space environment, such as ultra-high vacuum, high temperatures, cryogenic temperatures, space radiation, *etc.*,[1–3] lubricants are easily wasted and degraded. Once the lubricants wear down, the space hardware will seize and fail, preventing any further functionality. There are already many suitable lubricants for the space environment, including solid lubricants and liquid lubricants. Traditional solid lubrication materials, including graphite, MoS_2-based composite coatings, soft metal coatings (Pb, In, Au, Ag), polymer-based composites (PTFE and PEEK), and liquid lubricants involving perfluoropolyethers (PFPE), multi-alkylated cyclopentanes (MACs), *etc.*, were previously reported as the predominant lubricating material used for space technology.[4–6] However, whether for solid lubricants or liquid lubricants, there are always insurmountable shortcomings.[6,7] As space technology advances and demand for mechanical parts increases, so will lubrication requirements. From the National Aeronautics and Space Administration (NASA) report, currently no lubricant and coating exists or has been validated that meets such requirements. To meet the demand, additional research for potentially superior lubricants must be conducted.

Currently, diamond-like carbon films (DLC) are often referenced as potential space lubricating materials due to their high hardness, low friction, and low wear.[8–13] Hydrogenated DLC films have a low friction coefficient in vacuum. In the pioneering work of Enke *et al.*[14] friction coefficient values of 0.005–0.02 were measured when hydrogenated DLC films were sliding against steel in vacuum conditions ($p_{H_2O} = 10^{-8}$ Torr). Donnet *et al.*[15] measured the friction coefficient values in the range 0.006–0.008 for steel balls sliding against a-C:H film in vacuum. However, in long duration, heavily loaded, and high sliding speed applications, graphitization of DLC film, as well as adhesion and cold-welding between the DLC film and the counterpart easily occur under high vacuum conditions, resulting in a large friction coefficient, especially for the non/low hydrogenated DLC film.[16,17] Fortunately, new DLC-based composite solid–liquid lubricating coatings have been studied recently in space applications.[18] The research discovered that DLC/ionic liquid (DLC/IL) composite coatings have good performance in high vacuum and space radiation environments.[19] IL as a new potential space lubricant possesses extremely low vapor pressures, viability over large temperature ranges, excellent thermal stability and high electrical conductivity, which give it particular advantages in space-based applications.[20–22] However, the carrying capacity of

[a]State Key Laboratory of Solid Lubrication, Lanzhou Institute of Chemical Physics, Chinese Academy of Sciences, Lanzhou 730000, P.R. China. E-mail: Lpwang@licp.cas.cn; Fax: +86-09314968163; Tel: +86-09314968080

[b]The College of Chemistry and Chemical Engineering, Yibin University, Yibin 644000, P.R. China

liquid lubricants is limited, because liquid lubricants can undergo rheological thinning under high loads. Therefore, IL combined with a hard DLC film can minimize this weakness, and better suit it to higher load applications. However, the friction coefficient and wear resistance of DLC/IL coatings under high vacuum conditions are a little high,[18,19] so further improvement of the tribological performance for this kind of new composite coatings is required.

Additives are one way to improve existing lubricants, and they can supplement properties in which the lubricant is deficient. Graphene is a flat monolayer with two-dimensional sp^2 carbon atoms arranged in a honeycomb lattice,[23,24] and also is the building block of the solid lubricant graphite. The fundamental physical properties, including mechanical strength, tensile stress, thermal conductivity and aspect ratio, of graphene make it a suitable candidate for additives, namely, that it appears to be heat resistant, durable, and can provide a low coefficient of friction.[25,26] Graphene-based additives for base oil have already been studied to improve the load-carrying capacity and antiwear ability of lubricants in atmospheric environments.[27–30] The research indicates that graphene can significantly lower the friction coefficient and increase lubricant lifetime. However, studies of graphene-based additives for ionic liquids have been seldom reported,[22,26] and have remained a great interest to researchers in the pursuit of obtaining high bearing capacity and low-friction in space applications.

In this paper, we first prepared composite lubrication coatings consisting of IL with graphene-based additives and DLC film (DLC/IL/graphene), and evaluated their potential performance as space lubricants. We conducted our research on a self-made ground based simulation facility for high vacuum friction tests and space radiation friction tests. The hard film of DLC plays a major role in load bearing, while the IL can improve the ability of plasticity-resistant deformation of the substrate and reduce the friction coefficient. Moreover, graphene-based additives added into the ionic liquid can further improve the carrying capacity and friction-reducing ability. Based on this idea, the novel DLC/IL/graphene coating shows much promise for space applications.

2 Experimental

2.1 DLC film preparation

The DLC films used in this investigation were deposited on stainless steel substrates in an argon/methane atmosphere by an unbalanced magnetron sputtering technique. Prior to deposition, the stainless steel substrates were first ultrasonically cleaned in acetone for 20 min and then ultrasonically cleaned in alcohol for 10 min. After drying with dried gas, the samples were put into a deposition chamber. The base pressure of the deposition chamber was pumped down to 1.0×10^{-3} Pa, and then the chamber was backfilled with Ar gas of 100 sccm flow rate to 0.8 Pa. The substrates were cleaned using Ar^+ bombardment for 30 min at a substrate bias voltage of −1000 V to remove some adhering impurities on the substrates. Prior to the coating deposition, a Ti interlayer of about 150 nm with strong bonding to the substrates was deposited at a radio frequency (RF) power of 400 W, a bias voltage of −300 V and a duty cycle of 50%; then a-C:H film was deposited on the Ti interlayer at a bias voltage of −1000 V and a duty cycle of 20% in a flowing Ar + CH_4 atmosphere. The flow rate of Ar gas was 120 sccm, and the CH_4 was introduced into the system with an interval increment of 2 sccm per 2 minutes from 8 to 40 sccm at the beginning of the deposition, then the CH_4 remains constant. We did not heat during the deposition process, but the sample temperature was about 200 °C. Finally, the DLC film with a thickness of approximately 2 μm was successfully prepared on the stainless steel substrate. The nanohardness of the DLC film was measured by a Nanotest600 nanoindenter apparatus (MicroMaterials Ltd.) with a Berkovich diamond tip at a load of 50 mN and the indentation depth was about 10% of coating thickness to minimize the substrate contribution. The average hardness of the DLC film was approximately 20 GPa.

2.2 Preparation of graphene

Graphene oxide (GO) was synthesized from graphite powders according to the modified Hummers method.[31] In brief, 1 g of graphene powder was added to 98% H_2SO_4 (23 ml) in an ice bath. Then, 3 g $KMnO_4$ was slowly added to the mixture with constant stirring and the mixture was kept below 20 °C for 2 h after removal from the ice bath. Subsequently, 46 ml of distilled water was added to the mixture, which was immersed in a 98 °C water bath for 15 min. The mixture was then further diluted with deionized water (140 ml) and was treated with 30% H_2O_2 (12.5 ml). The resulting suspension was filtered, washed with dilute hydrochloric acid and distilled water, and dried at 50 °C to obtain GO. The GO was then dispersed in distilled water by ultrasonication to create a 1 mg ml^{-1} GO dispersion. Finally, 20 ml of 85% hydrazine mono-hydrate was added to 30 ml of the GO dispersion, and the mixture was treated at 50 °C for 12 h. After filtration, the graphene was obtained by washing with distilled water and dried at 50 °C.

2.3 Preparation of DLC/IL/graphene coatings

Firstly, an IL/graphene suspension of 0.125 mg ml^{-1} was prepared by mixing 6.25 mg graphene with 50 ml 1-butyl-3-methylimidazolium hexafluorophosphate ([BMIM][PF_6]) IL (the chemical formula is shown in Fig. 1a), which was synthesized by us following the similar procedures as proposed in a previous reference.[32] Probe sonication (SCIENTZ-II D 500W) was used for the dispersion of graphene in IL for 24 hours. Then this suspension was diluted to different concentrations of 0.025, 0.05, 0.075 and 0.01 mg ml^{-1}. Fig. 1b shows the photographs of different concentrations of stable and homogeneous IL/graphene nanofluids.

The IL/graphene nanofluids with different concentrations were coated on DLC films by spinning at 2000 rpm for 30 s. The thickness of the IL/graphene nanofluid layer was in a wide range of 0.5–2.0 μm. The interaction between the supporting layer of the solid DLC-based film and the upper liquid IL/graphene film was mainly physical adsorption. The DLC/IL/graphene solid–liquid lubricating coatings were successfully formed on steel for space performance characterizations.

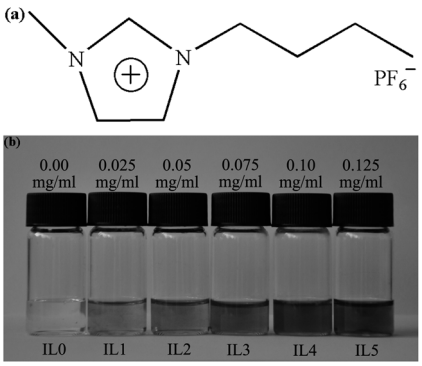

Fig. 1 (a) The chemical formulations of IL, (b) photographs of graphene-dispersed ionic liquid lubricants with different graphene concentrations.

2.4 Space properties characterizations

The space properties characterizations were composed of friction and wear tests under high vacuum and radiation environments. The friction and wear tests in high vacuum were performed on a self-made rotational ball-on-disk vacuum tribometer. The upper specimens were an AISI-52100 steel ball of standard 6 mm diameter, which was loaded against rotating discs. The rotational radius was set as 6 mm, the sliding speed was 500 rev per min and the normal load was 5 N. Two hour (corresponding to a total sliding distance of 2262 m) tests were performed at room temperature and under high vacuum (10^{-5} Pa) conditions. The friction coefficients were monitored continuously as a function of time. Each friction test was repeated three times under the same conditions in order to check the reproducibility of the measurements.

Atomic oxygen irradiation (AO), and ultraviolet irradiation (UV) experiments were carried out in ground based simulation facilities at Lanzhou Institute of Chemical Physics, Chinese Academy of Sciences. The basic principle schematic illustration of AO irradiation was outlined in ref. 33. The typical atomic oxygen flux at the sample position was determined to be 6×10^{15} atoms per cm^2 s^{-1}, and the exposure period was controlled at 120 min. The pressure of the UV irradiation test chamber was high vacuum on the order of 10^{-5} Pa, and the UV wavelength

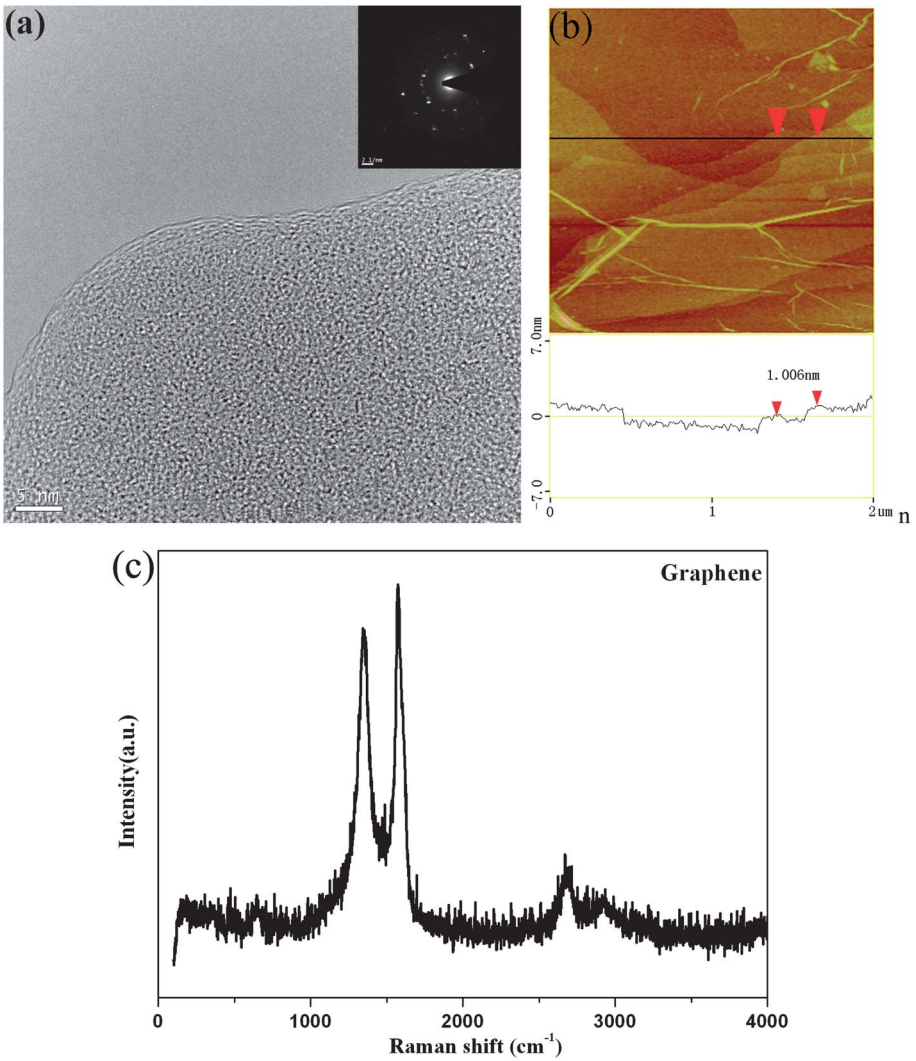

Fig. 2 (a) HRTEM of the graphene and the inset is the SAED pattern, (b) tapping-mode AFM height image of the graphene, (c) Raman spectra of the graphene.

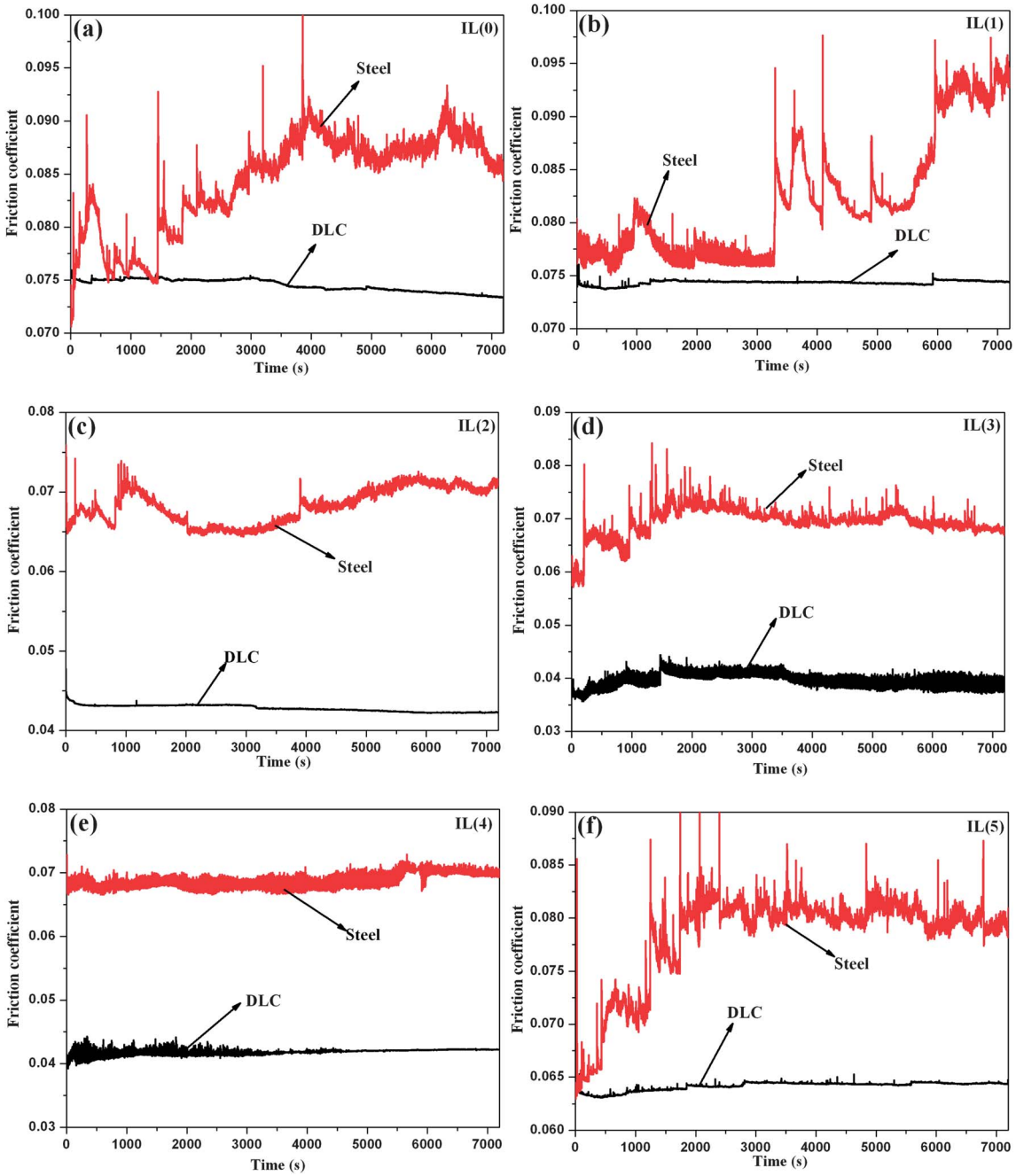

Fig. 3 Comparison of the tribological behaviors of the composite coatings of DLC/IL/graphene and steel/IL/graphene with different graphene concentrations sliding against a steel ball under high vacuum conditions: (a) IL0, (b) IL1, (c) IL2, (d) IL3, (e) IL4, and (f) IL5.

range was 115–400 nm. The typical UV energy flux at the sample position was determined to be about six times the solar constant, and the exposure period was controlled as 120 min, being equivalent to 12 sun hours. In the irradiation experiment process, DLC films and IL/graphene nanofluids were radiated separately. Before tribological testing, the radiated nanofluids were coated homogeneously on the radiated DLC films. The friction testing conditions were the same as the high vacuum conditions and each friction test was repeated three times under the same conditions in order to check the reproducibility of the measurements.

2.5 Characterizations of DLC/IL/graphene composite coatings

Graphene was characterized using high-resolution transmission electron microscopy (TECNAI TF20), multimode atomic force microscopy (AFM, Nanoscope IIIa, Veeco, and tapping mode), and Raman spectroscopy (Lab JY-HR800, Horiba, with 532 nm laser excitation). IL/graphene nanofluids with different concentrations were characterized by IR spectra which were recorded with a Nexus 870 infrared spectrometer using an attenuated total-reflection accessory (FTIRATR). The

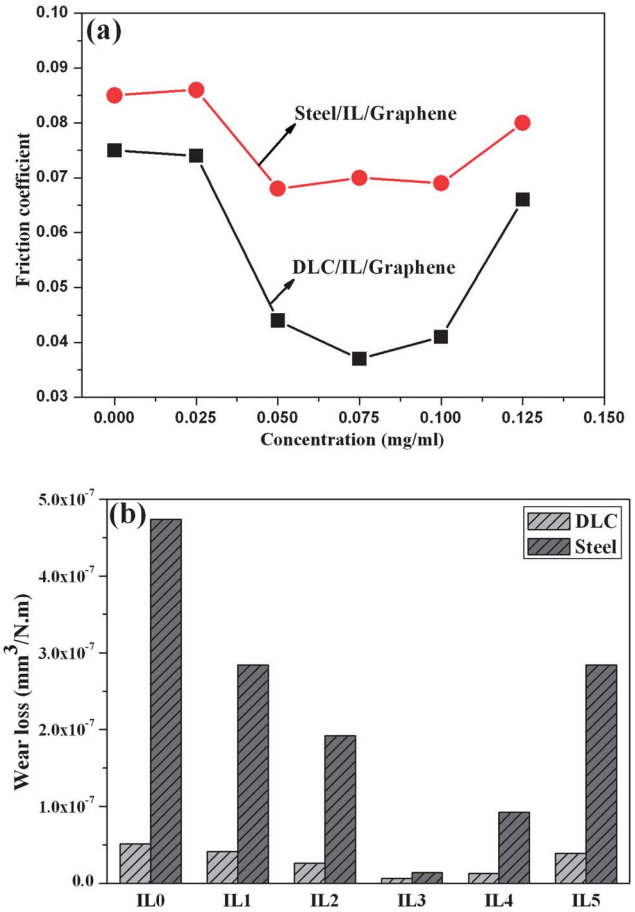

Fig. 4 (a) the average friction coefficient of the composite coatings of DLC/IL/graphene and steel/IL/graphene with different graphene concentrations and (b) the corresponding disc wear rates.

IL3 nanofluids before friction tests and on the wear track after friction tests were diluted in *N*,*N*-dimethyl formamide (DMF) by ultrasonic dispersion for a long time and the high resolution transmission electron micrograph and energy dispersive X-ray spectroscopy (EDX) analysis of graphene was carried out. The survey spectra, typical XPS spectra for different elements and chemical compositions of the IL/graphene nanofluids before and after tests were determined using an X-ray photoelectron spectroscope made by Thermon Scientific Company (XPS, K-Alpha-surface Analysis, X-ray Monochromatisation target). The wear track profiles and wear depth after the friction tests were obtained by a non-contact 3D surface profiler (model MicroMAXTM, made by ADE Phase Shift, Tucson, AZ, USA), and the disc wear rate was calculated by the wear depth.

3 Results and discussion

3.1 Characterization of graphene

Fig. 2a shows the typical high-resolution transmission electron microscopy (HRTEM) image and the corresponding selected area electron diffraction (SAED) pattern; the graphene is relatively smooth with sharp edges and ripples which is in agreement with previous reports.[34] Generally, the graphene layers can be distinguished by their folded edges.[35] As shown in Fig. 2a, the graphene is predominantly few-layer graphene with three to five layers. The SAED pattern of the few-layer graphene shows a clear six-fold pattern, revealing the graphitic crystalline nature of the graphene.[36] AFM is used to characterize the occasional monolayer graphene deposited on the freshly cleaved mica surface by drop-casting dilute graphene aqueous dispersions and by drying them at ambient temperature, as shown as Fig. 2b. The graphene with different lateral dimensions appears to overlap, which is a consequence of the sample deposition process; some thicker wrinkled regions are also presented on graphene, which enhances the surface roughness. The red marker corresponding to the average thickness of the monolayer graphene was around ~1 nm, which is larger than the theoretical thickness of pristine graphene (*i.e.*, 0.34 nm).[37] Fig. 2c gives the Raman spectrum of graphene. Graphene displays two prominent peaks, namely, the G band at 1568 cm^{-1} corresponding to the in-plane vibration of the sp^2-bonded carbon in a hexagonal lattice and the D band at 1345 cm^{-1}, which is associated with the vibration of disordered sp^3-hybridized carbon because of in-plane defects.[38] The 2D peak at 2676 cm^{-1} originates from a two phonon double resonance process. The shape and position of the 2D band identified the graphene as graphene nanosheets with few layers.[39] Based on the above-mentioned characterizations, graphene nanosheets were prepared successfully.

3.2 Space tribological properties of DLC/IL/graphene

We investigated the space performance of DLC/IL/graphene composite coatings in simulated environments, including the friction and wear properties under high vacuum and radiation environments. Fig. 3 depicts the friction curves of the composite coatings of DLC/IL/graphene and steel/IL/graphene with different graphene concentrations, sliding against a steel ball under high vacuum conditions. We could see that the friction curves of DLC/IL/graphene were much smoother, and the friction coefficient (COF) was more stable and lower as compared with that of steel/IL/graphene. Fig. 4 gives the corresponding average COF and the disc wear rates of the DLC/IL/graphene and steel/IL/graphene composite coatings. We could observe clearly that the average COF and disc wear rates of DLC/IL/graphene decreased gradually with increasing graphene content when the graphene concentration was below 0.075 mg ml^{-1}. As the graphene concentration increased beyond 0.075 mg ml^{-1}, the average COF and disc wear rates of DLC/IL/graphene increased with the graphene content. In other words, the COF and disc wear rates of DLC/IL3/graphene were the lowest of all. The average COF and disc wear rates of steel/IL/graphene had basically a similar trend. We also observed that the average COF and disc wear rates of DLC/IL/graphene were much lower than that of steel/IL/graphene, which indicated that the hard DLC film plays the role of load-bearing, and can effectively improve the friction-reduction and abrasion resistance. As shown in Fig. 4, the average COF of DLC/IL3 (0.075 mg ml^{-1}) was 0.037, which was just half as much as that of DLC/IL0 (no graphene, $\mu \sim 0.075$), and the disc wear rate of DLC/IL3/graphene was 6.61×10^{-9} mm^3 N^{-1} m^{-1}, which was about 1 order

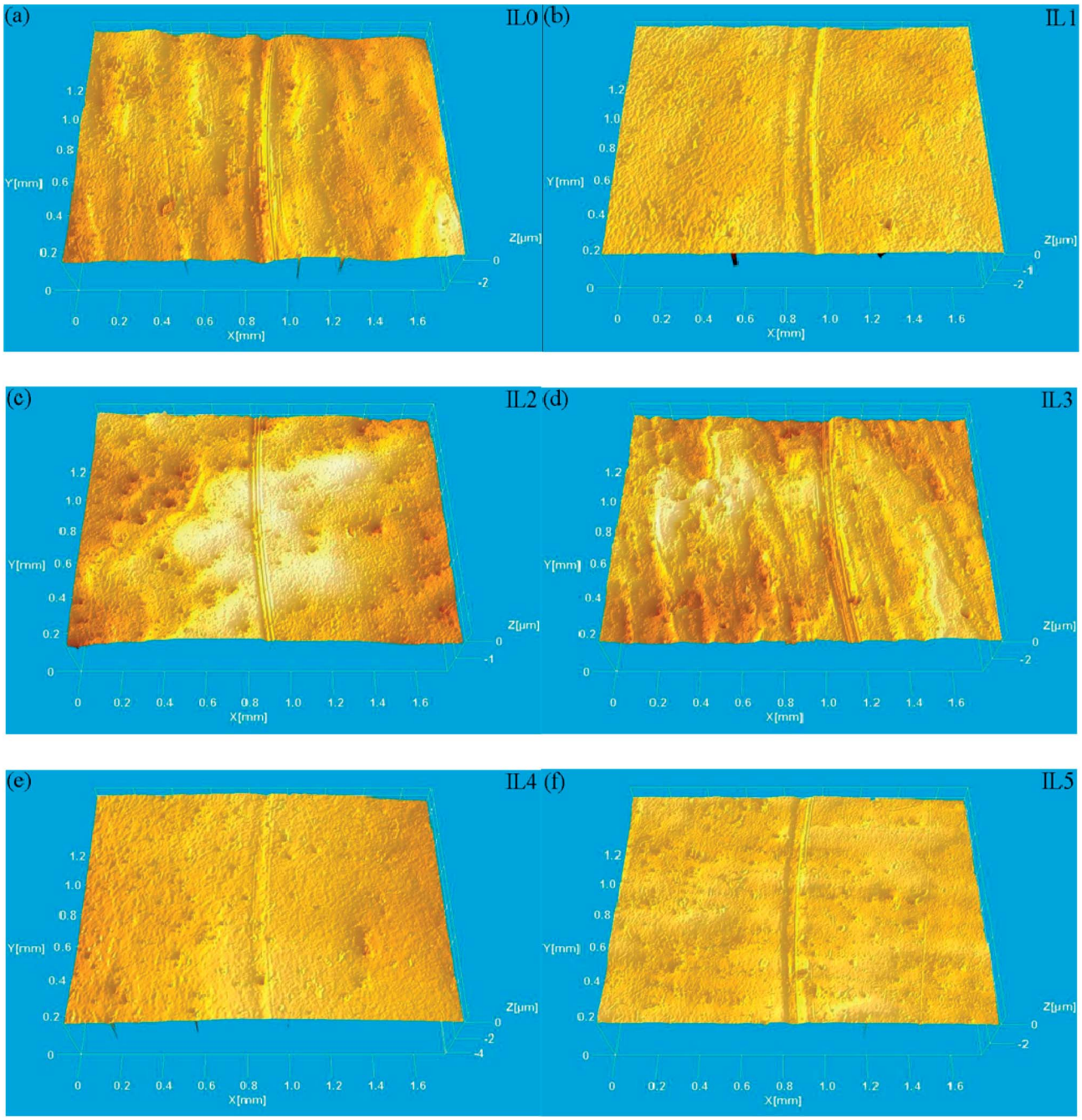

Fig. 5 The non-contact 3D surface profiler images of DLC/IL/graphene coatings from IL0 to IL5 in high vacuum.

of magnitude smaller than that of DLC/IL0/graphene (5.51×10^{-8} mm^3 N^{-1} m^{-1}). Moreover, the average COF and disc wear rates for all coatings containing graphene from IL1 to IL5 were always lower than that of IL0 without graphene addition, not only for the DLC/IL/graphene, but also for the steel/IL/graphene. These results indicated that the graphene additive added into IL could further enhance the friction-reduction and anti-wear ability of the composite coatings. Fig. 5 gives the non-contact 3D surface profiler images of the DLC/IL/graphene coatings from IL0 to IL5 in high vacuum conditions. Small and narrow wear tracks were shown on the DLC films. No significant plastic deformation was observed on the DLC films for all wear tracks, which could be attributed to the synergetic lubrication mechanism by the combination of the solid lubrication effect of the DLC-based film and the boundary lubrication of the liquid lubricant.

Fig. 6 presents the friction curves of DLC/IL/graphene (IL0, IL3 and IL4) before and after AO and UV irradiation under high vacuum conditions and the corresponding disc wear rates. The COF and disc wear rates after AO and UV irradiation were all much larger than that before irradiation, except for the COF of IL0 after UV irradiation, and the COF and disc wear rates after

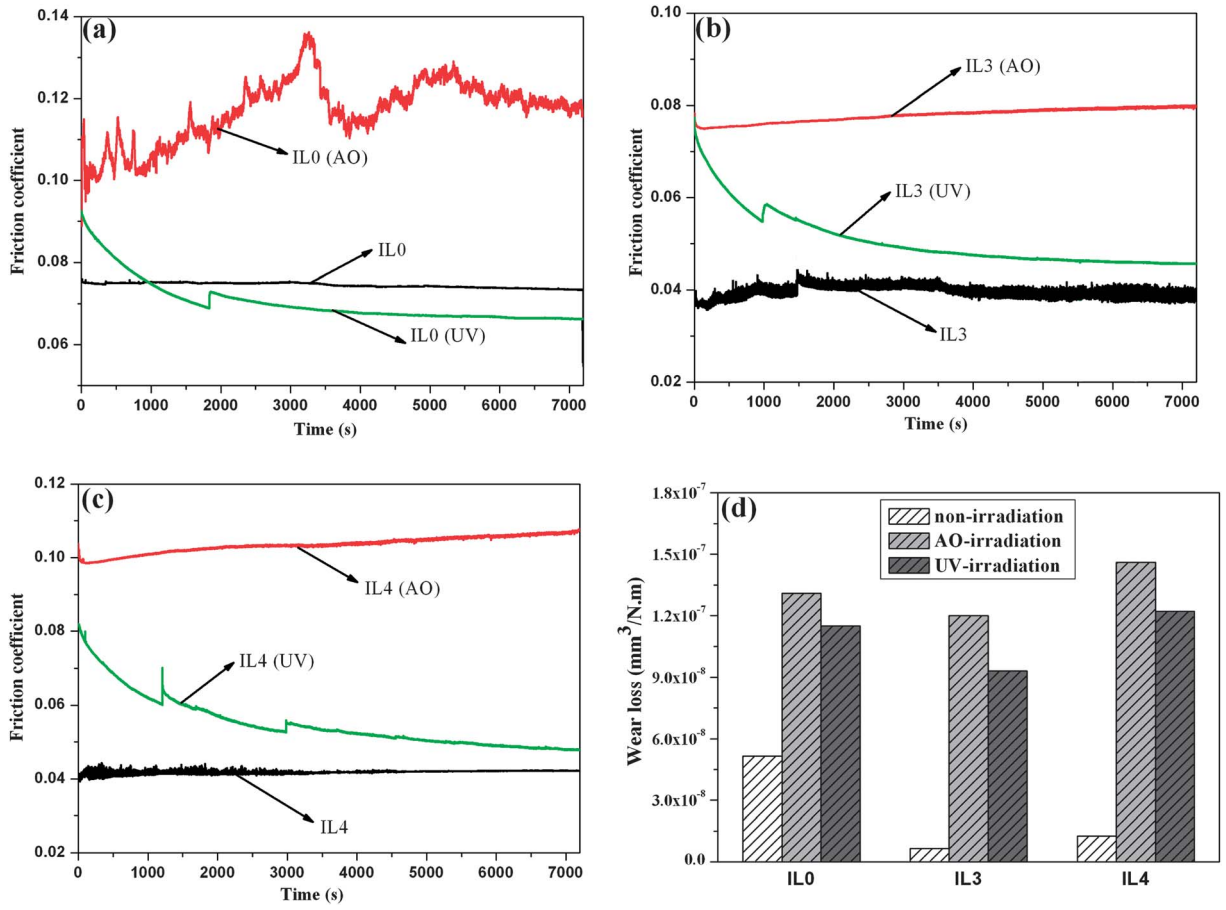

Fig. 6 Comparison of the tribological behaviors of the combination of DLC/IL/graphene before and after AO and UV irradiation under high vacuum conditions: (a) IL0, (b) IL3, (c) IL4, and (d) the corresponding disc wear rates.

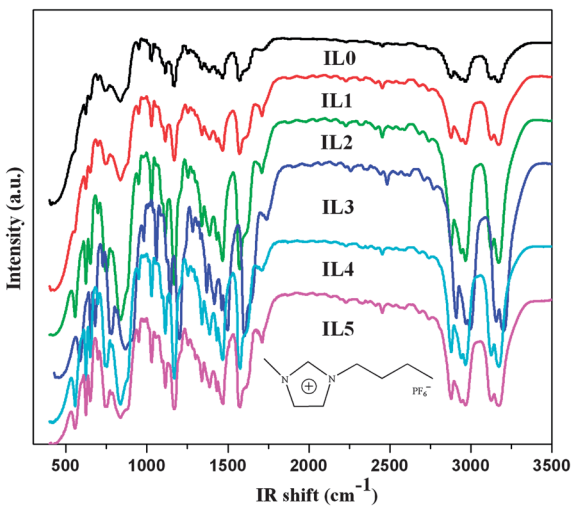

Fig. 7 The FTIR-ATR spectra of IL/graphene nanofluids with different graphene concentrations and the molecular formula of [BMIM][PF_6].

UV irradiation were lower than that after AO irradiation. These results indicated that the DLC film and IL/graphene nanofluids were damaged to different degrees by AO and UV irradiation and the destructive effect of AO irradiation was much stronger than that of UV irradiation.[19] Under the radiation environment, DLC/IL3/graphene (0.075 mg ml^{-1} graphene) showed the lowest COF and disc wear rates, which indicated that IL3 possesses the most powerful anti-radiation ability in this experiment. From the above results, it was concluded that there was an optimum concentration of graphene in IL for improving the friction-reduction and anti-wear ability of the DLC/IL/graphene composite coatings, and the optimum graphene concentration in IL was 0.075 mg ml^{-1}.

3.3 Characterization of IL/graphene nanofluids before and after tests

Furthermore, in order to get further information, the structure and composition of the IL/graphene nanofluids before and after tests in simulated space environments were investigated with FTIR, XPS spectra and TEM. Fig. 7 shows the FTIR-ATR spectra of the IL/graphene nanofluids with different graphene contents, and the molecular formula of [BMIM][PF_6]. It was clear that the typical characteristic peaks of [BMIM][PF_6] at 3169 cm^{-1} to 2929 cm^{-1} (symmetrical stretching vibration of alkyl chain), 1573 cm^{-1}(C–C and C–N stretching vibrations of the imidazolium ring), 1464 cm^{-1} to 1340 cm^{-1} (symmetrical deformation vibrations of alkyl chain), 1170 cm^{-1} to 1020 cm^{-1} (in-plane

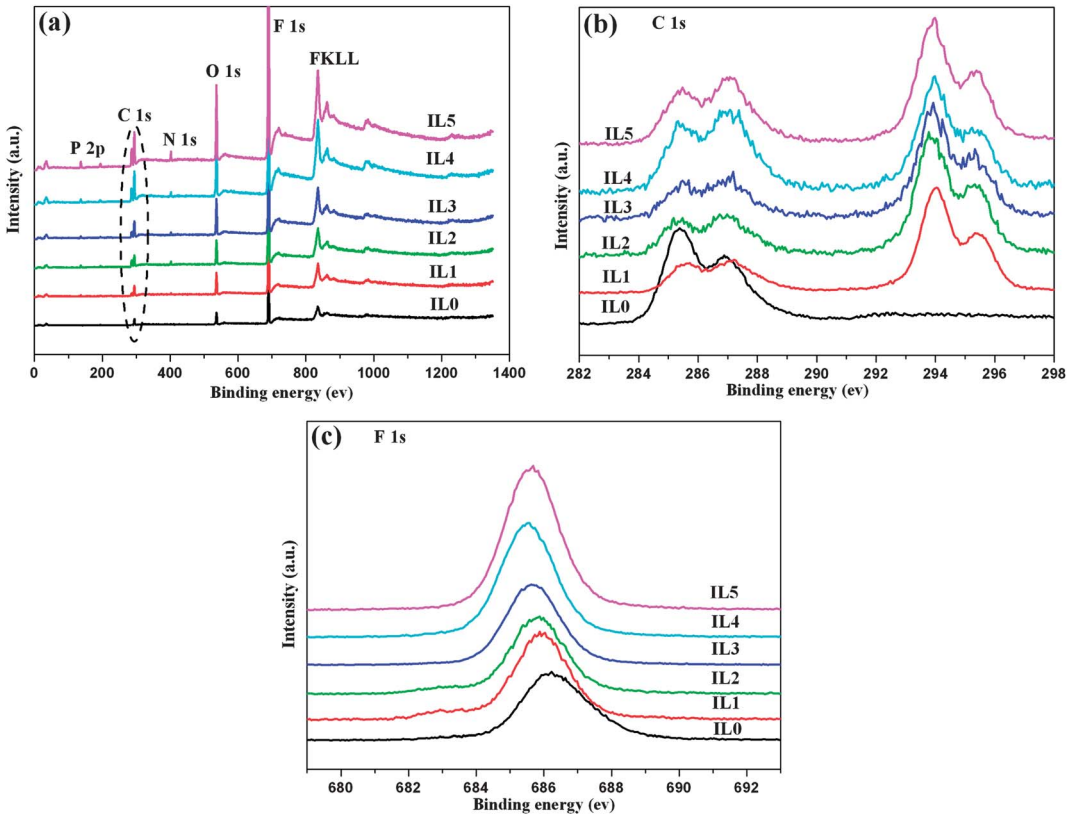

Fig. 8 XPS spectra of IL/graphene nanofluids with different graphene concentrations before tests: (a) survey spectra, (b) C 1s spectra, and (c) F 1s spectra.

wagging vibrations of alkyl chain), 800 cm^{-1} to 600 cm^{-1} (out-of-plane C–H bending vibrations of imidazolium ring), 820 cm^{-1} (the stretching vibration of PF_6^-) appeared in the IR spectra of all IL/graphene nanofluids.[40] As shown in Fig. 7, the wavenumbers of the characteristic peaks of the IL/graphene nanofluids were almost identical for different graphene concentrations, but the intensities of the characteristic peaks changed with the addition of graphene under the same measurement conditions. The intensities of the characteristic peaks became stronger with the increase of graphene concentration. Nevertheless, when the graphene concentration is up to 0.10 mg ml^{-1}, the intensities of the characteristic peaks began to reduce slightly. Based on these results, it was conjectured that the characteristic peak intensities could be affected by the concentration of graphene. There was a limit to which the graphene is dispersed in IL, and the optimum dose of graphene dissolved in IL is 0.075 mg ml^{-1}. If graphene was added into IL excessively, the excess graphene in IL would tended to form irreversible agglomerates and led to a reduction of the effective graphene dose, resulting in changes in the structure and performance of IL/graphene nanofluids.

More direct evidence for the changes in the IL/graphene nanofluids after space tribology tests was obtained from XPS spectra. Fig. 8 gives the XPS survey spectra, C 1s spectra and F 1s spectra of IL/graphene nanofluids with different graphene concentrations from IL0 to IL5 before tests. As shown in Fig.8a, XPS peaks of F 1s, C 1s, N 1s and P 2p were observed obviously in these survey spectra. As can be seen in the dotted area, the intensities of the C 1s band are enhanced gradually with increasing graphene concentration from IL0 to IL5. Fig. 8b gives the C 1s spectra from IL0 to IL5, respectively. The C 1s spectrum of IL0 was clearly different from the other C 1s spectra. There were only two peaks arising from the C 1s XPS spectrum for IL0, where the peak at 285.3 eV was assigned to the CH_2 group in the alkyl chain of IL, while the second peak at 286.8 eV might originate from the C atoms bonded to the N atoms (C*–N in imidazolium ring).[41] From IL1 to IL5, two distinct C groups were revealed in the C 1s XPS spectra: (i) the lower binding energy group, which consisted of two peaks, was assigned to CH_2 and C*–N in IL and graphene; (ii) the higher binding energy group, which also consisted of two peaks between 292 eV and 296 eV, was assigned to the CF_2 group.[42] The two groups were quite obvious in the C 1s spectra from IL1 to IL5. It was indicated that some of the C atoms and F atoms formed weak bonds and generated CF_2 groups during sonication. Fig. 8c presents the F 1s spectra from IL0 to IL5. There was one peak for all ILs, but the peak positions were different from IL0 to IL5. The F 1s peak of IL0 appeared at 686.2 eV, which was attributed to the PF_6^- group. The F 1s shifted to 685.9–685.4 eV for IL1–IL5. This suggested that the PF_6^- anion began to decompose after the graphene was added into IL.[43] In the F 1s spectrum, C–F peaks did not appear. It was possible that only a few PF_6^- anions decomposed when the graphene was added into IL and the C–F bonds were very weak.

Fig. 9 shows the XPS C 1s spectra, F 1s spectra and Fe 2p spectra of IL/graphene nanofluids with different graphene

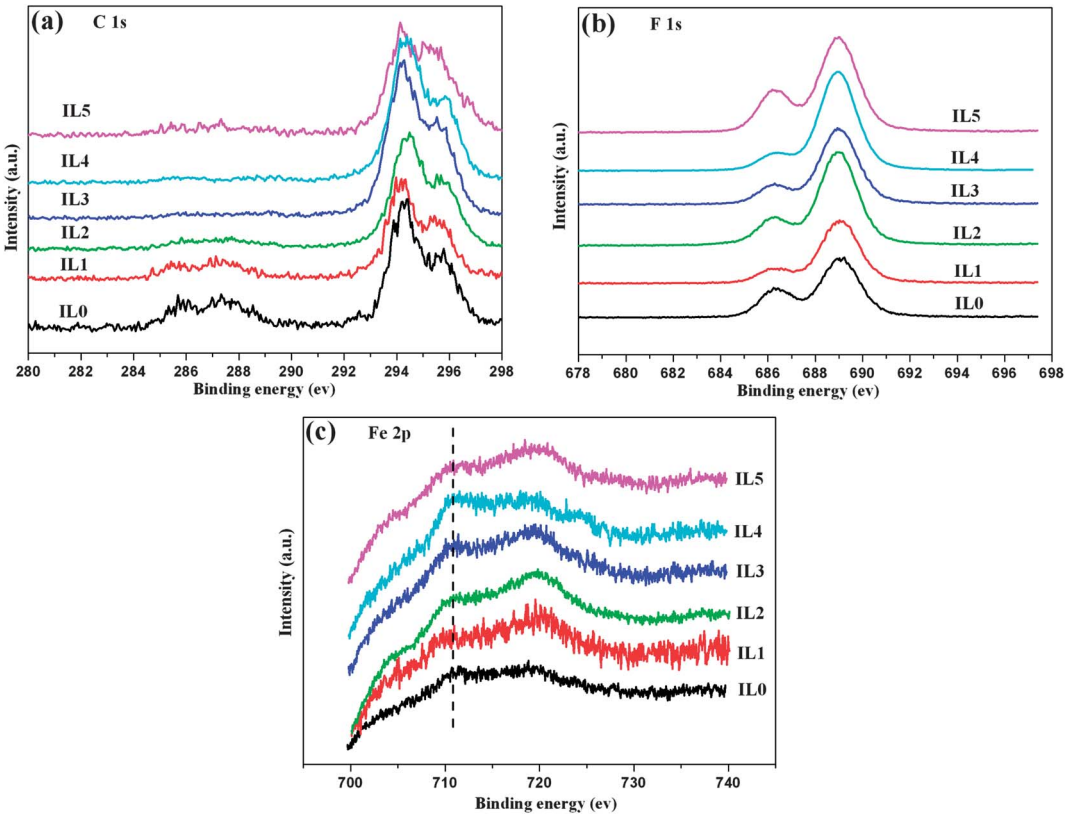

Fig. 9 XPS spectra of IL/graphene nanofluids with different graphene concentrations after friction testing under high vacuum conditions: (a) C 1s spectra, (b) F 1s spectra, and (c) Fe 2p spectra.

concentrations from IL0 to IL5 after friction testing in high vacuum. As can be seen from Fig. 9a, the intensity of the peaks for the (ii) group became stronger, which were assigned to the CF_2 group. Nevertheless, the peaks for the (i) group, which were attributed to CH_2 and C–N in imidazolium rings, alkyl chains and graphene, became weaker and even disappear. There was only a weak (i) peak for IL0, IL1, IL2 and IL5, and this peak for IL0 was the strongest, but for IL3 and IL4, this peak disappeared. The possible reason was that the C–F bonds are generated pervasively in the IL/graphene nanofluids after friction testing in high vacuum, and the intensity of the C–F peaks was so strong that other peaks were weakened and even disappeared. The CF_2 peaks also appeared for IL0 after friction testing in spite of no graphene being added to it. This was because wear debris of the DLC film was doped into IL0 and the carbon element might bind with the F element. Fig. 9b gives the F 1s spectra from IL0 to IL5. The peaks of F 1s after friction testing were quite different from those before friction testing. Each F 1s spectrum after friction testing had two distinct peaks at about 686.1 eV and 688.9 eV. The higher binding energy peak was associated with C–F bonds which were adsorbed onto the surface. The lower binding energy peak at about 686.1 eV was consistent with fluoride, like Fe fluoride and PF_6^-.[42] The counterparts were the steel ball with a diameter of 6 mm, therefore Fe was detected by XPS analysis in the IL/graphene nanofluids after friction tests. The Fe 2p peaks at 710.8 eV, as shown in Fig. 9c, correspond to FeF_2, FeF_3, $FePO_4$, and ferric oxide.[44]

Fig. 10 provides the XPS C 1s and F 1s spectra of the IL/graphene nanofluids of IL0, IL3 and IL4 after AO and UV radiated friction tests. As shown in Fig. 10a, these two groups of C peaks after radiated friction tests were much stronger when compared with those for non-irradiation (Fig. 8b). Tables 1 and 2 present the two groups of C ((i) and (ii)) relative atomic concentration of IL0, IL3 and IL4 before and after AO and UV radiated friction tests, and the ratio of them. The ratio values of (i)/(ii) after radiated friction tests made a dramatic increase when compared with those after friction tests in high vacuum. Furthermore, the ratio values of (i)/(ii) after AO radiated friction tests were much larger than those after UV radiated friction tests and high vacuum friction tests. As can be seen from Tables 1 and 2, the ratio value of IL3 after UV irradiation tests was the closest to that before tests. Combined with these results, we investigated the possible reason. Under AO and UV irradiation, some weak bonds including the F element in the IL lubricant were broken, then formed some small fluorine-containing molecules by oxidation reaction and being gasified to surrounding circumstances.[19] Thus, the generation of C–F decreased with the reduction of F atoms, and so did the relative atomic concentration of the C–F group, leading to an increase in the ratio values of (i)/(ii). Fig. 10b shows the F 1s spectra after radiated friction tests. As compared with Fig. 9b, these two F peaks become stronger after radiated friction tests. The enhancement of lower band energy peaks indicated the increase in Fe fluorides. It suggested that the corrosiveness of IL toward

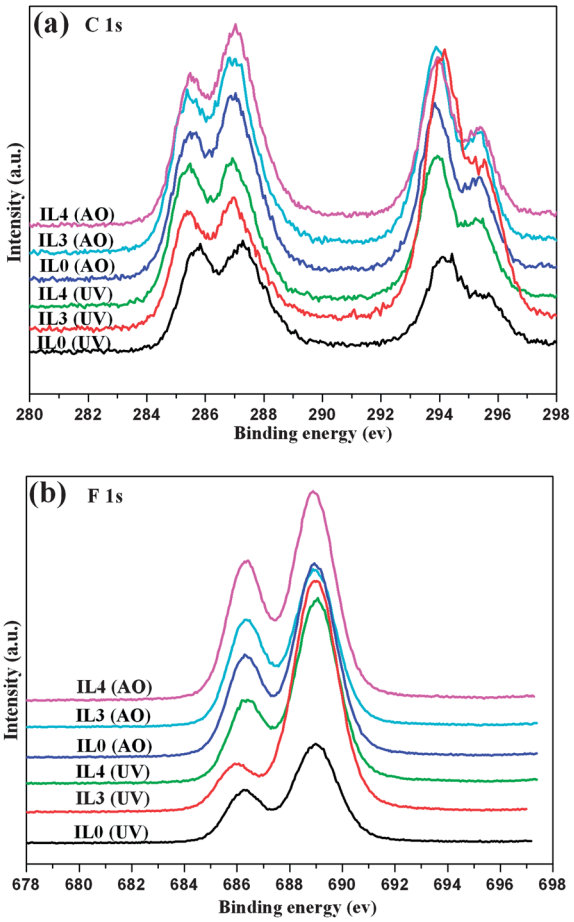

Fig. 10 XPS spectra of IL/graphene nanofluids of IL0, IL3 and IL4 after AO and UV irradiation and friction tests: (a) C 1s spectra and (b) F 1s spectra.

Table 1 Two groups of C relative atomic concentration (at%), in which (i) presents the lower binding energy (CH_2 and C–N in imidazole ring and alkyl chain) and (ii) presents the higher binding energy (C–F bonds) for IL0, IL3 and IL4 for non-irradiation, and the ratio of them

	IL0[a]	IL0[b]	IL3[a]	IL3[b]	IL4[a]	IL4[b]
(i) (at%) (CH_2, C–N)	20.67	2.5	11.49	—	18.42	0.54
(ii) (at%) (C–F)	—	24.92	22.11	27.32	17.27	25.87
(i)/(ii)	∞	0.10	0.52	0	1.07	0.02

[a] Before friction tests. [b] After friction tests in high vacuum.

the counterpart steel ball could be enhanced after irradiation. As analysed in Fig. 10, Tables 1 and 2, the ratio values of (i)/(ii) after UV radiated friction tests are all lower than those after AO irradiated friction tests. Meanwhile, the C 1s and F 1s spectra of IL3 had minimal changes compared with the others after radiated friction tests, and the ratio values of (i)/(ii) for IL3 after UV radiated friction testing was quite close to that before friction tests. These results indicated that the destructive effect of AO irradiation was much stronger than that of UV irradiation, and the IL3 nanofluid exhibits the strongest anti-radiation capacity.

We selected an optimum concentration of IL3 before and after high vacuum friction tests to dilute in DMF by ultrasonic dispersion for a long time and carry out the HRTEM of graphene. Fig. 11a presents the HRTEM images of graphene before friction tests. The graphene sheet showed a crinkled morphology, which was characteristic of the graphene obtained from the chemical reduction route.[45] When the IL/graphene nanofluid was diluted in DMF by ultrasonic dispersion for a long time, we could clearly observe that the graphene sheets were clean and spotless. Fig. 11b shows the HRTEM images of graphene after high vacuum friction tests. The morphology of the graphene sheets after friction tests was greatly different to that before tests. The lamellar graphene sheets were spotted with many black specks, because some IL particles were sandwiched between the graphene sheets. EDX analysis was carried out in this area with many black specks, as shown in Fig.11c. The characteristic elements of IL, such as N, P and F, appeared in this EDX spectrum, and further proved the existence of IL among the graphene sheets. The Cu element was attributed to the copper mesh used in TEM detection. These results also suggested that after long time friction tests in high vacuum, IL intermingled into the graphene sheets and generated some chemical reactions with graphene.

3.4 Friction and wear mechanism of DLC/IL/graphene

In order to determine the mechanism responsible for the ultralow-friction and excellent anti-wear behavior of the DLC/IL/graphene composite coatings, we designed a simple friction and wear mechanism schematic, as shown in Fig. 12. Firstly, graphene was stably and homogeneously dispersed in ionic liquid by ultrasonic dispersion for a long time, as shown in Fig. 12a. In this process, graphene might react with active groups or activated atoms of IL.[46,47] XPS spectra showed that C–F peaks existed in the C 1s spectra after graphene was dispersed in IL, but the intensity of this peak was relatively weak (Fig. 8b). Moreover, there were no C–F peaks in the F 1s spectra for the IL/graphene nanofluids (Fig. 8c). It was indicated that C–F bonds were generated in the IL/graphene nanofluids, but they were few in number and the C–F bonds were so weak that they

Table 2 Two groups of C relative atomic concentration (at%), in which (i) presents the lower binding energy (CH_2 and C–N in imidazole ring and alkyl chain) and (ii) presents the higher binding energy (C–F bonds) for IL0, IL3 and IL4 after AO and UV irradiated friction testing, and the ratio of them

	IL0 (AO)	IL0 (UV)	IL3 (AO)	IL3 (UV)	IL4 (AO)	IL4 (UV)
(i) (at%) (CH_2, C–N)	20.88	20.31	18.67	11.04	20.55	19.75
(ii) (at%) (C–F)	13.37	13.43	14.10	18.52	12.72	14.05
(i)/(ii)	1.56	1.51	1.32	0.60	1.62	1.41

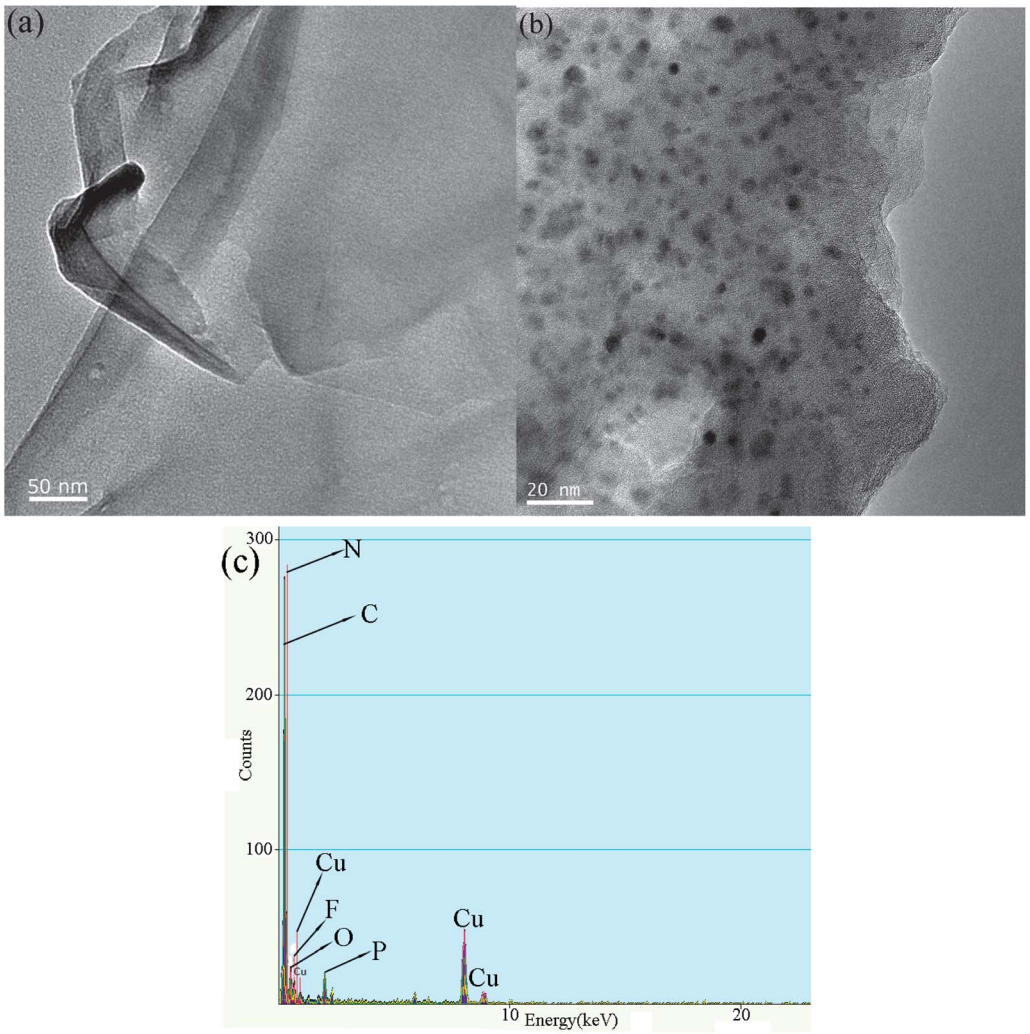

Fig. 11 High-resolution transmission electron micrograph (HRTEM) of graphene obtained by diluting IL3 in DMF (a) before friction testing, (b) after friction testing, (c) the corresponding EDX analysis of (b).

were eliminated by diluting in DMF and ultrasound for a long time (Fig. 11a). Then, the IL/graphene nanofluids were coated onto the DLC films and formed DLC/IL/graphene composite coatings. The DLC/IL/graphene composite coatings slid against a steel ball with high speed and high load under high vacuum conditions, as shown in Fig. 12b. It was reported that formation of a transfer layer on the counterpart is the key to friction reduction and wear resistance for DLC-based composite coatings.[48] For the DLC/IL composite coatings without graphene, formation of a transfer layer depends on the mixture of the wear debris and the oil, so the wear debris of the DLC film is the key factor, and the transfer layer could form after a period of friction sliding. However, for the DLC/IL/graphene composite coatings, the situation is not exactly the same. Graphene dispersed into IL can easily accumulate in the area between the composite coatings and the counterpart steel ball by sliding towards one direction, which contributed to formation of the early transfer layer before wear debris formed (Fig. 12c). Furthermore, due to the superior lubricating properties of IL, in the primary stage of DLC/IL/graphene friction, there was no running-in stage and the friction coefficient was very low and stable due to the existence of graphene. Through repetitious sliding, wear debris increased gradually and mixed with IL/graphene, forming a compact, dense and continuous tribofilm on the surface of the counterpart (Fig. 12d). Moreover, we can observe in the inset of Fig. 12d, due to the repetitious sliding in high vacuum, more C–F bonds were generated in the surface of the IL/graphene nanofluids, and the C–F bonds was so strong that they cannot be eliminated by diluting in DMF and by ultrasound for a long time (Fig. 11b). In other words, two fluorinated surfaces were generated on the surfaces of the wear track and wear scar. These results had been already proved by XPS in Fig. 9. It was reported that surface fluorination could decrease the surface energy and reduce the friction and wear.[49] In actuality, the fluorinated oil-containing carbon-rich tribofilms were formed between the friction pairs and improve the friction-reduction and anti-wear ability of the composite coating significantly. Meanwhile, the formation of fluoride iron on the surface of the counterpart steel ball (shown as Fig. 9c) could also effectively improve the wear resistance. Moreover, under high vacuum conditions,

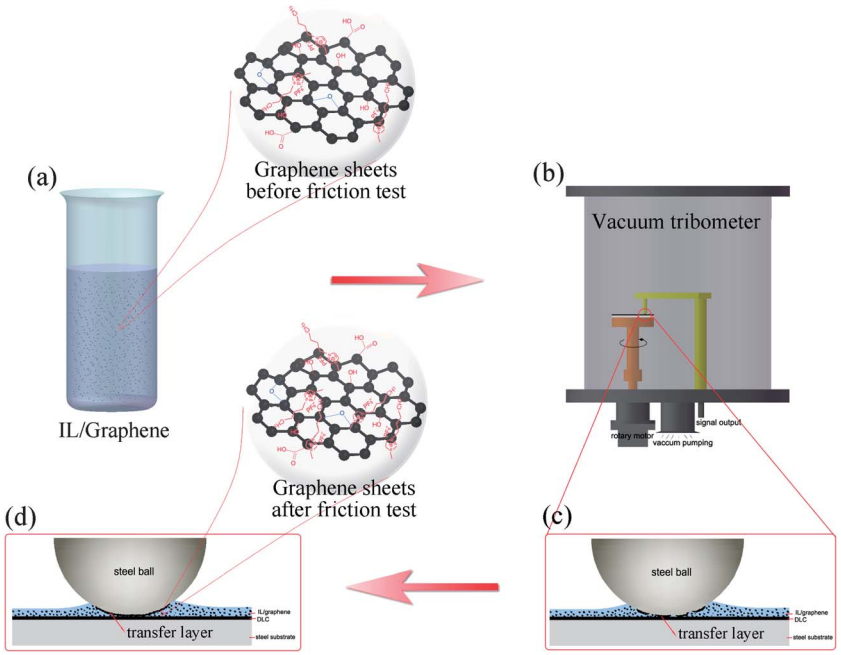

Fig. 12 Schematic to explain the possible friction and wear mechanism for the DLC/IL/graphene composite coatings in high vacuum conditions.

when the friction movement was towards one direction, fluoride iron would not be eliminated.[50–52] We also found that the friction performance did not always improve with increasing graphene addition. The friction coefficient was lowest when the graphene concentration was 0.075 mg ml^{-1} (IL3). It was indicated that there was an optimum dose of graphene dissolved into IL. If excess graphene was added into IL, graphene would tend to form irreversible agglomerates, leading to a reduction of the effective graphene dose, and it could not stably and homogeneously disperse in IL. Therefore, the optimum amount of graphene as a lubricant additive can effectively improve the space performance, including high vacuum and irradiated environments.

4 Conclusion

We successfully prepared stable and homogeneous dispersions of IL/graphene nanofluids with different graphene concentrations and DLC/IL/graphene composite coatings. The space performances, including the friction and wear properties in high vacuum and under irradiated environment, were investigated in this paper. The results showed that the tribological performance did not always improve with the increase in graphene addition, and the DLC/IL3 (0.075 mg ml^{-1} graphene) exhibited the best friction-reducing and anti-wear performances, both in high vacuum and in a radiated environment. This suggested that there would be an optimum dispersion capacity of graphene dispersed into IL. We also investigated the friction and wear mechanism of the DLC/IL/graphene composite coatings in high vacuum conditions. An early transfer layer was easily formed due to the existence of graphene, so a very low and stable friction coefficient was observed at the beginning of the friction test. The formation of fluorinated oil-containing carbon-rich tribofilms between the friction pairs further ensured the capacity for friction-reduction and wear-resistance in high vacuum and irradiated environment of the DLC/IL/graphene composite coatings. The DLC/IL/graphene composite coatings have great potential for the development of applications in space in the future.

Acknowledgements

This work was supported by the National Natural Science Foundation of China (no. 51105352 and no. 11172300).

Notes and references

1 X. H. Zhao, Z. G. Shen, Y. S. Xing and S. L. Ma, *Polym. Degrad. Stab.*, 2005, **88**, 275.
2 H. Y. Sang, W. J. Zhang and T. M. Wang, *Vacuum*, 2003, **68**, 203.
3 J. Rao, K. J. Lawson and J. R. Nicholls, *Surf. Coat. Technol.*, 2005, **197**, 154.
4 M. R. Hilton and P. D. Fleischauer, *Surf. Coat. Technol.*, 1992, **54–55**, 435.
5 W. Hübner, T. Gradt, T. Schneider and H. Börner, *Wear*, 1998, **216**, 150.
6 W. R. Jones Jr and M. J. Jansen, Space tribology, NASA/TM-2000–209924.
7 K. Miyoshi, Solid lubricants and coatings for extreme environments: state-of-the-art survey, NASA/TM-2007–214668.
8 S. G. Zhou, L. P. Wang, Z. B. Lu, D. Qi, S. C. Wang, R. J. K. Wood and Q. J. Xue, *J. Mater. Chem.*, 2012, **22**, 15782.
9 C. Donnet, *Surf. Coat. Technol.*, 1996, **80**, 151.

10 Y. X. Wang, L. P. Wang, S. C. Wang, G. A. Zhang, R. J. K. Wood and Q. J. Xue, *Tribol. Lett.*, 2010, **40**, 301.
11 L. P. Wang, S. H. Wan, S. C. Wang, R. J. K. Wood and Q. J. Xue, *Tribol. Lett.*, 2010, **38**, 155.
12 S. G. Zhou, L. P. Wang and Q. J. Xue, *Tribol. Lett.*, 2010, **43**, 329.
13 S. H. Yang, H. Kong, K.-R. Lee, S. J. Park and D. E. Kim, *Wear*, 2002, **252**, 70.
14 K. Enke, H. Dimigen and H. Hübsh, *Appl. Phys. Lett.*, 1980, **36**, 291.
15 C. Donnet, M. Belin, J. C. Auge, J. M. Martin, A. Grill and V. Patel, *Surf. Coat. Technol.*, 1994, **68–69**, 626.
16 S. Miyake, S. Takahashi, I. Watanabe and H. Yoshihara, *ASLE Trans.*, 1987, **30**, 121.
17 J. Fontaine, T. L. Mogne, J. L. Loubet and M. Belin, *Thin Solid Films*, 2005, **482**, 99.
18 X. F. Liu, L. P. Wang and Q. J. Xue, *Wear*, 2011, **271**, 889.
19 X. F. Liu, L. P. Wang, J. B. Pu and Q. J. Xue, *Appl. Surf. Sci.*, 2012, **258**, 8289.
20 M. Palacio and B. Bhushan, *Adv. Mater.*, 2008, **20**, 1194.
21 W. Morales, K. W. Street, V. R. Koch and R. M. Richard, *Prox. 62nd Annual Meeting of the STLE*, Philadelphia, Pa, 2008.
22 J. B. Pu, S. H. Wan, W. J. Zhao, Y. F. Mo, X. Q. Zhang, L. P. Wang and Q. J. Xue, *J. Phys. Chem. C*, 2011, **115**, 13275.
23 K. S. Novoselov, A. K. Geim, S. V. Morozov, D. Jiang, Y. Zhang, S. V. Dubonos, I. V. Grigorieva and A. A. Firsov, *Science*, 2004, **306**, 666.
24 A. K. Geim and K. S. Novoselov, *Nat. Mater.*, 2007, **6**, 183.
25 C. Lee, X. Wei, J. W. Kysar and J. Hone, *Science*, 2008, **321**, 385.
26 K. W. Street, W. Morales and R. L. van der Wal, Application of carbon based nano-materials to aeronautics and space lubrication, 2007, NASA/TM–;2007–214473.
27 H. D. Huang, J. P. Tu, L. P. Gan and C. Z. Li, *Wear*, 2006, **261**, 140.
28 T. Filleter, J. L. McChesney, A. Bostwick, E. Rotenberg, K. V. Emtsev, T. Seyller, K. Horn and R. Bennewitz, *Phys. Rev. Lett.*, 2009, **102**, 086102.
29 J. S. Lin, L. W. Wang and G. H. Chen, *Tribol. Lett.*, 2011, **41**, 209.
30 V. Eswaraiah, V. Sankaranarayanan and S. Ramaprabhu, *ACS Appl. Mater. Interfaces*, 2011, **3**, 4221.
31 W. S. Hummers Jr and R. E. Offeman, *J. Am. Chem. Soc.*, 1958, **80**, 1339.
32 J. D. Holbery and K. R. Seddon, *J. Chem. Soc., Dalton Trans.*, 1999, 2133.
33 L. Ji, H. Li, F. Zhao, W. Quan, J. Chen and H. Zhou, *Appl. Surf. Sci.*, 2009, **255**, 4180.
34 F. Günes, H. J. Shin, C. Biswas, G. H. Han, E. S. Kim, S. J. Chae, J. Y. Choi and Y. H. Lee, *ACS Nano*, 2010, **4**, 4595.
35 N. Li, Z. Y. Wang, K. K. Zhao, Z. J. Shi, Z. N. Gu and S. K. Xu, *Carbon*, 2010, **48**, 255.
36 C. Nethravathi, T. Nisha, N. Ravishankar, C. Shivakumara and M. Rajamathi, *Carbon*, 2009, **47**, 2054.
37 H. F. Yang, C. S. Shan, F. H. Li, D. X. Han, Q. X. Zhang and L. Niu, *Chem. Commun.*, 2009, 3880.
38 A. C. Ferrari, J. C. Meyer, V. Scardaci, C. Casiraghi, M. Lazzeri, F. Mauri, S. Piscanec, D. Jiang, K. S. Novoselov and S. Roth, *Phys. Rev. Lett.*, 2006, **97**, 187401.
39 T. Y. Kim, H. W. Lee, J. E. Kim and K. S. Suh, *ACS Nano*, 2010, **4**, 1612.
40 F. Shi and Y. Q. Deng, *Spectrochim. Acta, Part A*, 2005, **62**, 239.
41 S. L. Ren, S. R. Yang, Y. P. Zhao, T. Yu and X. D. Xiao, *Surf. Sci.*, 2003, **546**, 64.
42 J. H. Sanders, J. N. Cutler and G. John, *Appl. Surf. Sci.*, 1998, **135**, 169.
43 Z. G. Mu, F. Zhou, S. X. Zhang, Y. M. Liang and W. M. Liu, *Tribol. Int.*, 2005, **38**, 725.
44 M. H. Yao, M. J. Fan, Y. M. Liang, F. Zhou and Y. Q. Xia, *Wear*, 2010, **268**, 67.
45 B. Zhang, W. Ning, J. Zhang, X. Qiao, J. Zhang, J. He and C.-Y. Liu, *J. Mater. Chem.*, 2010, **20**, 5401.
46 Y. L. Min, K. Zhang, L. H. Chen, Y. C. Chen and Y. G. Zhang, *Synth. Met.*, 2012, **162**, 827.
47 V. H. Pham, H. D. Pham, T. T. Dang, S. H. Hur, E. J. Kim, B. S. Kong, S. Kim and J. S. Chung, *J. Mater. Chem.*, 2012, **22**, 10530.
48 X. F. Liu, L. P. Wang and Q. J. Xue, *Surf. Coat. Technol.*, 2011, **205**, 2738.
49 K. Trojan, M. Grischke and H. Dimigen, *Phys. Status Solidi A*, 1994, **145**, 575.
50 D. J. Carre and J. A. Makowitz, *ASLE Trans.*, 1985, **28**, 40.
51 D. J. Carre, *ASLE Trans.*, 1986, **29**, 121.
52 S. Mori and W. Morales, *Tribol. Trans.*, 1990, **33**, 325.